Super Enhancer-Mediated Upregulation of *HJURP* Promotes Growth and Survival of t(4;14)-Positive Multiple Myeloma

Yunlu Jia[1,2], Jianbiao Zhou[1,3], Tze King Tan[1], Tae-Hoon Chung[1], Yongxia Chen[4], Jing-Yuan Chooi[3], Takaomi Sanda[1,3], Melissa J. Fullwood[1,5], Sinan Xiong[3], Sabrina H.M. Toh[1], Kalpnaa Balan[1], Regina W.J. Wong[1], Julia S.L. Lim[1], Enfan Zhang[6], Zhen Cai[6], Peng Shen[2], and Wee Joo Chng[1,3,7]

ABSTRACT

Multiple myeloma is an incurable malignancy with marked clinical and genetic heterogeneity. The cytogenetic abnormality t(4;14) (p16.3;q32.3) confers aggressive behavior in multiple myeloma. Recently, essential oncogenic drivers in a wide range of cancers have been shown to be controlled by super-enhancers (SE). We used chromatin immunoprecipitation sequencing of the active enhancer marker histone H3 lysine 27 acetylation (H3K27ac) to profile unique SEs in t(4;14)-translocated multiple myeloma. The histone chaperone *HJURP* was aberrantly overexpressed in t(4;14)-positive multiple myeloma due to transcriptional activation by a distal SE induced by the histone lysine methyltransferase *NSD2*. Silencing of *HJURP* with short hairpin RNA or CRISPR interference of SE function impaired cell viability and led to apoptosis. Conversely, *HJURP* overexpression promoted cell proliferation and abrogated apoptosis. Mechanistically, the NSD2/BRD4 complex positively coregulated *HJURP* transcription by binding the promoter and active elements of its SE. In summary, this study introduces SE profiling as an efficient approach to identify new targets and understand molecular pathogenesis in specific subtypes of cancer. Moreover, *HJURP* could be a valuable therapeutic target in patients with t(4;14)-positive myeloma.

Significance: A super-enhancer screen in t(4;14) multiple myeloma serves to identify genes that promote growth and survival of myeloma cells, which may be evaluated in future studies as therapeutic targets.

Introduction

Multiple myeloma is a malignancy of postgerminal center B-lineage cells with marked chromosomal heterogeneity in biologic and clinical presentation. Worldwide, multiple myeloma is the second most common blood cancer and results in over 100,000 deaths per year (1). Multiple myeloma remains an incurable disease, with most patients experiencing relapse and requiring new therapeutic approaches (2). Chromosomal translocations and enhancers hijacking by variable genes (*MYC*, *MAF*, *CCND1/2/3*, *NSD2*) are recognized oncogenic driver events during myeloma pathogenesis (3, 4). Four chromosomal partners were revealed to account for a majority of immunoglobulin heavy-chain (*IgH*) translocations: 11q13 (*cyclin D1*), 6p21 (*cyclin D3*), 4p16 (*FGFR3* and *NSD2*), and 16q23 (*c-MAF*; ref. 5). Among these, the t(4;14) (p16.3;q32.3) translocation, occurring in 15% to 20% of presenting myeloma cases, fuses the *NSD2* and *FGFR3* gene to the *IgH* promoter/enhancer, leading to the overexpression of these two genes (6). Patients with multiple myeloma with t(4;14) have an inferior outcome and do not respond well to cytotoxic chemotherapy (7, 8).

Transcriptional dysregulation is among the most frequent events in cancer pathogenesis. The altered transcriptional programs cause cancer cells to become addicted to continuous and robust transcription of certain oncogenes (9, 10). Recently, genome regions consisting of active-enhancer clusters together to form super-enhancers (SE), have been reported to be essential for controlling key genes to specify cell identity (11, 12). Compared with typical enhancers (TE), SEs cover a larger genomic span with extra-high levels of histone H3 lysine 27 acetylation (H3K27ac) binding, and are more densely occupied by master transcription factors, chromatin regulators, and mediator proteins (13, 14). Indeed, malfunction of SEs and SE-driven oncogene transcription during malignant transformation and progression is a general mechanism in nearly all human cancers (15–17). Cancer-specific SE profiling has also been employed to search for novel oncogenes and potential therapeutic targets.

THZ1 is a covalent inhibitor of cyclin-dependent kinase 7 (CDK7; ref. 18). Recent studies have identified a subset of aggressive cancers

[1]Cancer Science Institute of Singapore, National University of Singapore, Centre for Translational Medicine, Singapore, Republic of Singapore. [2]Department of Medical Oncology, the First Affiliated Hospital, Zhejiang University School of Medicine, Hangzhou, China. [3]Department of Medicine, Yong Loo Lin School of Medicine, National University of Singapore, Singapore, Republic of Singapore. [4]Department of Surgical Oncology, Sir Run Run Shaw Hospital, Zhejiang University School of Medicine, Hangzhou, China. [5]School of Biological Sciences, Nanyang Technological University, Singapore, Republic of Singapore. [6]Bone Marrow Transplantation Center, the First Affiliated Hospital, Zhejiang University School of Medicine, Hangzhou, China. [7]Department of Hematology-Oncology, National University Cancer Institute of Singapore (NCIS), The National University Health System (NUHS), Singapore, Republic of Singapore.

Note: Supplementary data for this article are available at Cancer Research Online (http://cancerres.aacrjournals.org/).

Y. Jia, J. Zhou, and T.K. Tan contributed equally to this article.

Corresponding Author: Wee Joo Chng, Department of Haematology-Oncology, National University Cancer Institute of Singapore (NCIS), The National University Health System (NUHS), 1E, Kent Ridge Road, Singapore 119228. Phone: 656-772-4613; Fax: 656-777-5545; E-mail: mdccwj@nus.edu.sg

Cancer Res 2022;82:406–18

doi: 10.1158/0008-5472.CAN-21-0921

with exceptional sensitivity to CDK7 inhibition, including triple-negative breast cancer, (19) lung cancer, (20) MYCN-dependent neuroblastoma (21), and esophageal squamous cell carcinoma (22). The vulnerability of these malignancies to CDK7 inhibition was reported to be mediated by SE-driven oncogenic transcriptional dependencies. Previously, using an integrative analysis of identifying SE landscape by high-throughput H3K27ac chromatin immunoprecipitation (ChIP) platform followed by further filtering those SE-associated genes whose expression are significantly downregulated following THZ1 treatment, we have identified several functionally relevant SE-associated genes in T-cell acute lymphoblastic leukemia and myeloma cells (23, 24). Using a similar strategy, we seek to identify SE-associated genes of functional relevance in t(4;14) myeloma and understand how they are regulated.

Materials and Methods

Cell culture and reagents

The human multiple myeloma cell lines LP-1, OPM2, H929, KMS28BM, KMS11, RPMI8226, U266, KMS12 and Burkitt lymphoma cell lines Daudi and Raji were obtained from the ATCC. All of the cell lines were grown in RPMI-1640 medium (BioWest) supplemented with 10% FBS and 1% penicillin–streptomycin, and kept at 37°C with 5% CO_2. The identity of all cell lines was recently authenticated by short tandem repeat analysis. Plasma cells were isolated by CD138 immunomagnetic bead selection from bone marrow aspirates of newly diagnosed patients with multiple myeloma, obtained from the National University Hospital. The experimental protocol was established according to the ethical guidelines of the Helsinki Declaration, and was approved by the Human Ethics Committee of National University of Singapore. Written informed consent was obtained from individual or guardian participants. DMSO was purchased from Sigma. THZ1 (HY-80013) and JQ1 (HY-13030) were obtained from Cayman Chemical and Medchemexpress, respectively. All antibodies used are shown in Supplementary materials and methods.

SE peak calling and identification

SE regions were determined by calling peaks in H3K27ac (Abcam, ab4729) ChIP sequencing (ChIP-seq) data set as described previously, (24) then combining enhancers occurring within 12.5 kb of each other into a single larger domain based on the strategy used by Whyte and colleagues (12). Normalized reads for each region were ranked against the total number of peaks. Cut-off for SE designation was set at peaks with a tangent slope of more than 1. Library construction and sequencing on the Illumina HiSeq 4000 platform were performed by BGI Tech Solutions Co., Limited.

CRISPR construct design

CRISPR guide RNAs were designed using the CRISPR direct design tool (https://crispr.dbcls.jp/). Oligonucleotides corresponding to these identified target sequences were obtained from Integrated DNA Technologies Pte Ltd., Singapore and subcloned into the lent guide-blasticidin plasmid and infected into dCas9-KRAB stable-expressing cells. The CRISPR (Addgene, plasmid #71236) and inducible expression of guide RNA with fluorescent GFP reporter (Addgene, plasmid #70183) vectors were gifts from Takaomi Sanda. The sequences of the guide RNA (gRNA) target sites are as follows, with the protospacer adjacent motif (PAM) target sequence: holiday junction recognition protein (*HJURP*) gRNA-1, GGGGGTATTTGTACGCTACTGTT; *HJURP* gRNA-2, AGCTTTATCGCATTATGGACGTT; gRNA-3, CCCTTCTGTCCCAACG-TCAAGTT.

Circular chromosome conformation capture

Circular chromosome conformation capture sequencing (4C-seq) assays were performed as previously described in Werken and colleagues, (25) with slight modifications. Briefly, 4×10^7 cells were cross-linked with 1% formaldehyde (Sigma). The nuclei pellets were then isolated by cell lysis with cold lysis buffer (10 mmol/L Tris-HCl, 10 mmol/L NaCl, 5 mmol/L EDTA, 0.5% NP 40) supplemented with protease inhibitors (Roche). First-step digestion was performed overnight at 37°C with the EcoRI enzyme (NEB). After confirmation of good digestion efficiency by gel electrophoresis, DNA was ligated in dilution conditions by T4 DNA ligase (Thermo Fisher Scientific) and then subsequently de–cross-linked. After reversal of the cross-links, the DNA was extracted by phenol-chloroform to obtain a 3C library. This 3C library was then subjected to a second round of digestion with DpnII enzyme (NEB) and ligation, generating a 4C library. The 4C library DNA concentration was determined using Qubit assays (Thermo Fisher Scientific). The 4C library was then amplified using specific primers with Illumina Nextera adapters and sent for sequencing on the MiSeq platform. We used the Capture HiC Plotter (CHiCP), a web-based tool for the integrative and interactive visualization of promoter captures Hi-C (PCHi-C) datasets, to identify long-range interactions in the high-resolution capture Hi-C dataset of Mifsud and colleagues (26) from the LCL GM12878. A list of 4C primers was included in Supplementary Table S1.

Coimmunoprecipitation and Western blot analysis

Three days after transient transfection, KMS11 cells were harvested and washed with ice-cold PBS before being disrupted with lysis buffer (50 mmol/L Tris, 100 mmol/L NaCl, 0.1% NP-40, 50 mmol/L NaF, 1 mmol/L dithiothreitol, 1 mmol/L phenylmethylsulfonyl fluoride, 1 μg/mL of aprotinin, 0.5 μg/mL of leupeptin, and 0.7 μg/mL of pepstatin). One milligram of protein lysates was incubated with 5 μL of anti-BRD4 or anti-NSD2 antibody at 4°C for 4 hours, followed by the addition of 10 μL of protein G slurry (Santa Cruz Biotechnology) for 1 hour. Coimmunoprecipitation was performed using nuclear extract collected from KMS11 after washing with lysis buffer three times, and the immunoprecipitated protein was separated by SDS-PAGE and analyzed by Western blot.

Cell synchronization and immunofluorescence assay

H929 cells were transduced with scramble control and sh-*HJURP*#2 lentivirus for 72 hours, then proceeded to cell-cycle synchronization according to a published protocol (27). In brief, cells were sequentially treated with 4 mmol/L thymidine (Sigma, 1895) for 24 hours, washed and released into the standard medium for 9 hours, then incubated with 20 ng/mL nocodazole (Sigma, M1404) for 4 hours. The mitotic cells were washed and grown in normal for 20 minutes, then incubated with 50 mmol/L blebbistatin (Sigma, B0560). At a 10-minute interval up to 60 minutes, the harvested cells were cytospinned onto slides, fixed with 4% paraformaldehyde, then stained with CENP-A primary antibody (GeneTex, GTX13939) and mouse IgG1-Fluorescein secondary antibody (Sigma, SAB3701170). Coverslips were then mounted using the mounting medium with DAPI (Vectashield, H-1200). Images were captured with an LSM710 (Zeiss) confocal microscope.

Statistical analysis

Nonparametric statistics were used with Prism 5.0 software (Graphpad Software). Survival data were analyzed using the Kaplan–Meier method. A χ^2 test was performed to analyze the categorical correlation. Student t test and Mann–Whitney test were used to analyze parametric and nonparametric variables,

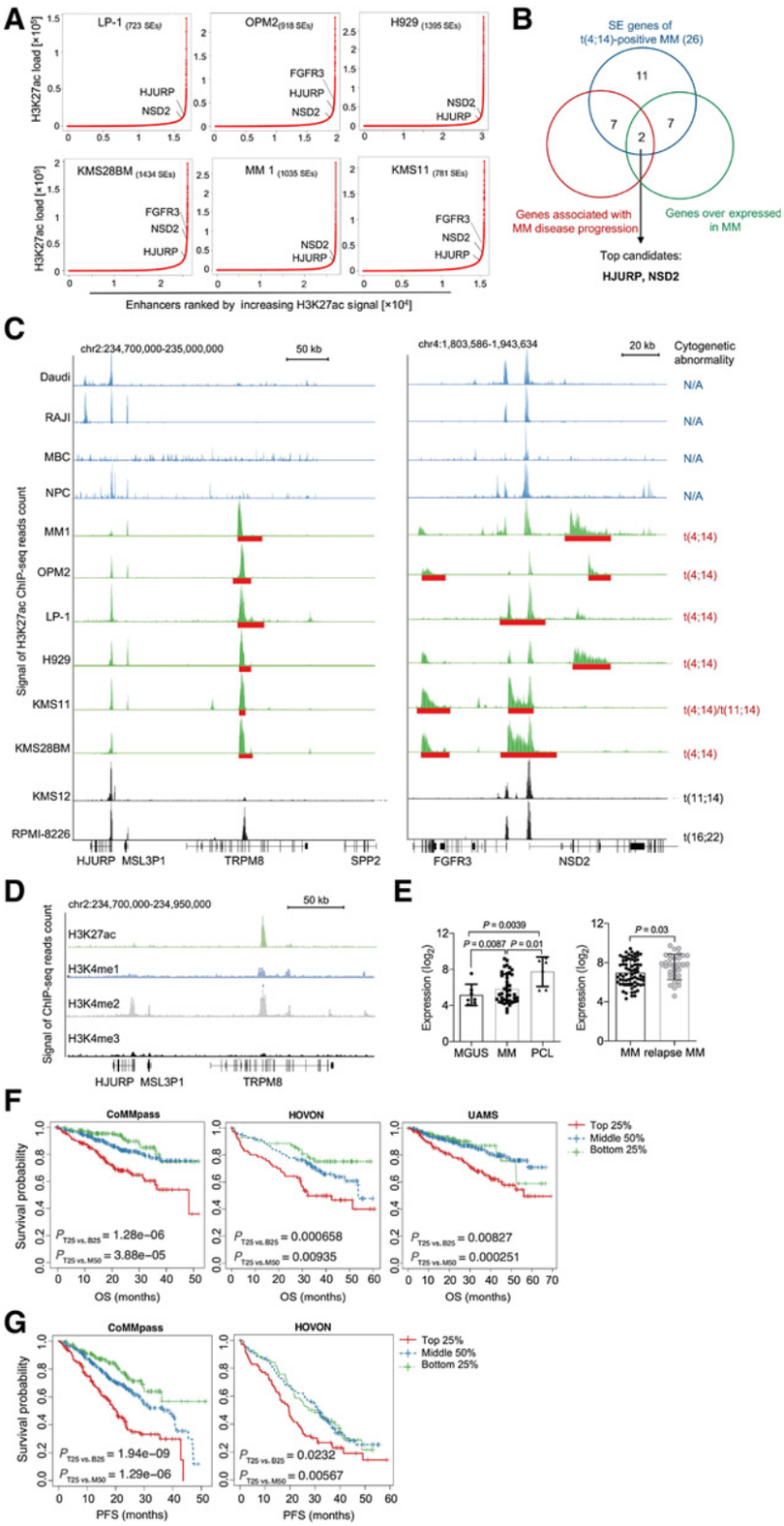

Figure 1.

Epigenomic enhancer profiling defined *HJURP* as an SE-associated gene of t(4;14)-positive multiple myeloma. **A,** Enhancer regions of HMCLs (LP-1, OPM2, H929, KMS28BM, and KMS11) and patient-derived multiple myeloma sample (MM 1) carrying t(4;14) translocation. Enhancers were ranked by increasing H3K27ac signal, and enhancers above the inflection point of the curve were defined as SEs, while the rest were TEs. The number of SEs are shown for each sample, and examples of SE-associated genes *HJURP*, *NSD2*, and *FGFR3* are also presented. **B,** Venn diagram of t(4;14) multiple myeloma–specific SE genes, genes associated with unfavorable survival of patients with multiple myeloma, and genes overexpressed in multiple myeloma showing some overlapping genes. *HJURP* and *NSD2* were identified as the top candidate SE-associated genes from the selection strategy. **C,** Gene tracks of H3K27ac ChIP-seq signal across t(4;14)-positive HMCLs, patient-derived myeloma tissue, and the control samples (Daudi, RAJI, MBC, and NPC) at the *HJURP*, *NSD2*, and *FRFG3* loci. **D,** ChIP-seq data tracks showing the enrichment of H3K27ac (green), H3K4me1 (blue), H3K4me2 (gray), and H3K4me3 (black) at the *HJURP* SE loci. The relatively increased enrichment of H3K4me1 to H3K4me3 was observed in the H3K27ac-enriched SE region, and high enrichment of H3K4me2 signal was indicated at both the distal and proximal regions of the *HJURP* gene. **E,** Based on Gene Expression Omnibus databases (GSE2113 and GSE6477), *HJURP* overexpression contributed to myelomagenesis with gradual increasing expression from monoclonal gammopathy of undetermined significance (MGUS), SMM to newly diagnosed and relapsed multiple myeloma or plasma cell leukemia **F**. Prognostic implications of *HJURP* expression profiles in patients with multiple myeloma carrying translocation t(4;14) or without t(4;14) in the CoMMpass, HOVON, and UAMS dataset, separately. **G,** The effect of *HJURP* expression on OS in patients with myeloma with or without t(4;14) in the CoMMpass and HOVON dataset, separately. Kaplan–Meier survival curves were compared by log-rank test. MM, multiple myeloma; PCL, plasma cell leukemia.

respectively. A *P* value less than 0.05 was considered statistically significant.

Data availability statements

All data generated or analysed during this study are included in the published article and its additional files. The ChIP-seq data have been deposited in the Gene Expression Omnibus database (accession number: gse145938)

Results

HJURP was identified as an SE-associated gene of t(4;14)-positive multiple myeloma

Using a well-established active enhancer mark, H3K27ac, we systematically profiled the landscape of active enhancers in a series of t(4;14)-positive human myeloma cell lines (HMCL; LP-1, OPM2, H929, KMS11, and KMS28BM) and one patient-derived multiple myeloma sample (MM 1; **Fig. 1A**). For the controls, we profiled the

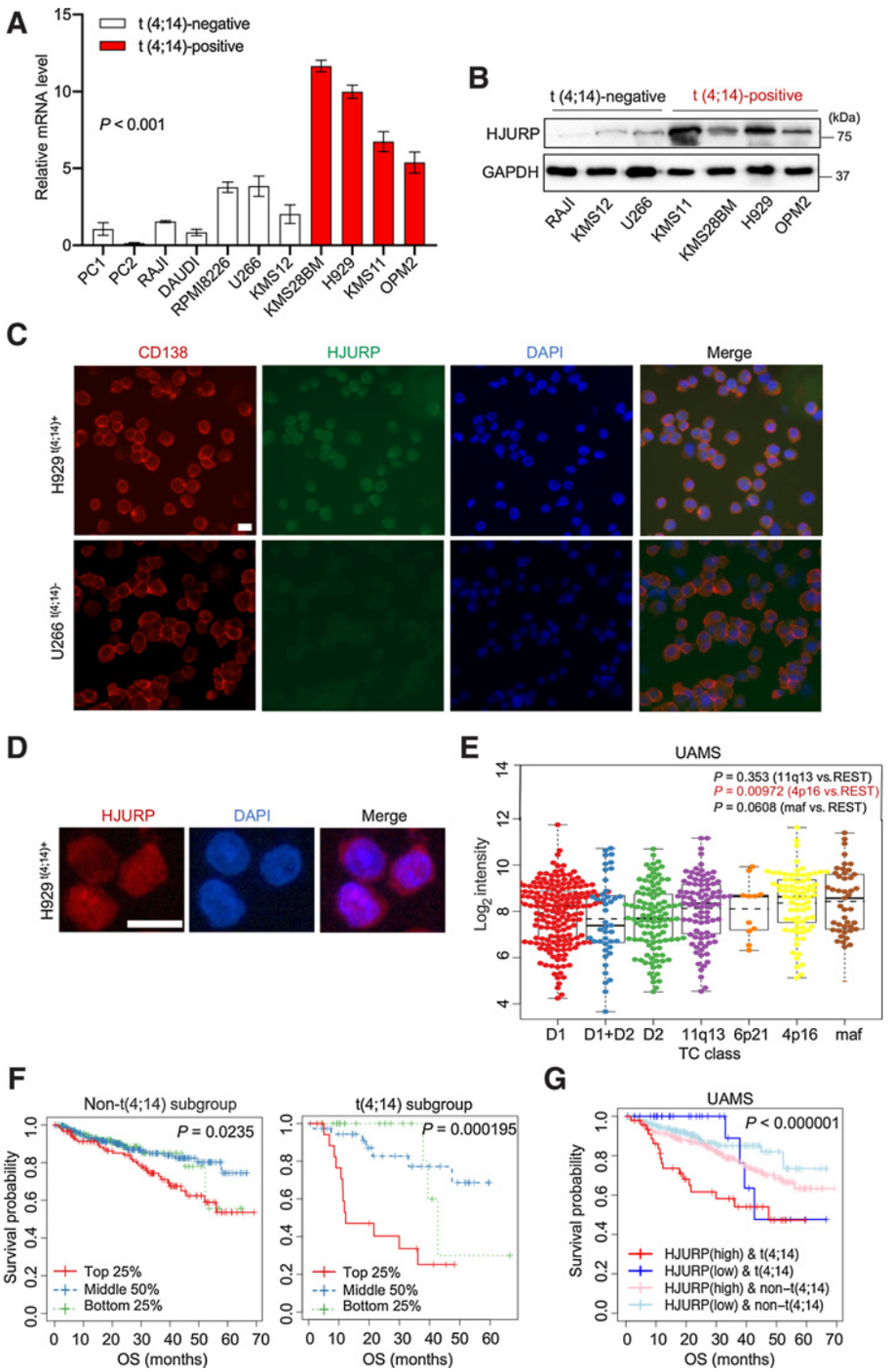

Figure 2.
Expression profiling and prognostic implication of *HJURP* in t(4;14) and non-t(4;14) myeloma cases. **A** and **B,** The mRNA (**A**) and protein (**B**) expression levels of *HJURP* were relatively elevated in t(4;14)-positive HMCLs compared with non-t(4;14) samples. Data are presented as the mean ± SD of three independent experiments. Significant differences between the t(4;14)-negative and t(4;14)-positive groups as determined by one-way ANOVA ($P < 0.0001$). **C,** HJURP (green) and CD138 protein (red) in H929 [t(4;14)-positive] and U266 [t(4;14)-negative] cells was determined with IF staining with DAPI (blue) counterstaining. Scale bars, 10 μm. **D,** IF assay detected that *HJURP* protein (red) mainly localized to the nucleoplasm & nucleoli in the t(4;14)-positive H929 cell. DNA (blue) was stained with DAPI. Scale bars, 10 μm. **E,** Expression levels of *HJURP* in a collection of multiple myeloma samples derived from the UAMS dataset. Upregulation of *HJURP* was observed in t(4;14) subgroup (4p16) compared with the rest ($P = 0.00972$). Student *t* tests were performed, and data are presented as mean ± SD. **F,** Prognostic implications of *HJURP* expression profiles in patients with multiple myeloma carrying translocation with t(4;14) or without t(4;14), separately. **G,** The effect of *HJURP* expression on OS in patients with myeloma with or without t(4;14). Kaplan–Meier survival curves were compared by log-rank test. TC, translocations/cyclins.

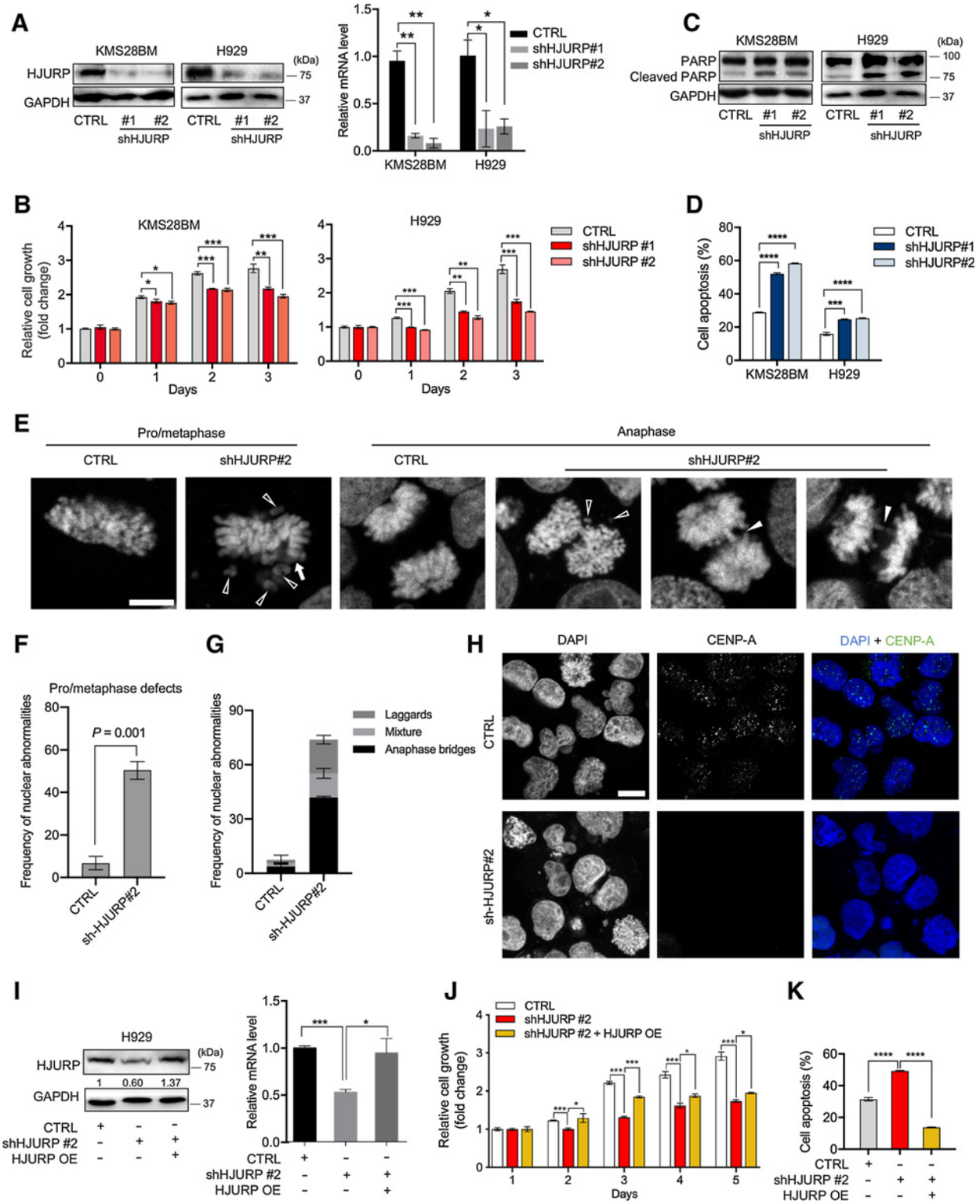

Figure 3.

Deletion of *HJURP* impaired multiple myeloma cell growth and induced apoptosis. **A,** Expression levels of *HJURP* protein and mRNA were detected upon *HJURP* shRNA transfection or the control vector in KMS28BM and H929 cells. **B,** Proliferation of KMS28BM and H929 cells was significantly inhibited upon *HJURP* silencing. The cell proliferation was tested every 24 hours using CTG assays. (*Continued on the following page.*)

epigenetic landscape of non-t(4;14) multiple myeloma cells (KMS12 and RPMI-8226), B-lymphoma cell lines (Daudi and RAJI), normal plasma cell (NPC), and memory B cell (MBC; Supplementary Fig. S1A; ref. 28). A total of 3,319 SE-associated genes were identified in all t(4;14) multiple myeloma samples, of which, 26 SE genes were commonly acquired in both HMCLs and patient-derived multiple myeloma sample (Supplementary Table S2). To prioritize these genes for further study, we selected SE-associated genes with the following criteria: (i) overlap with prognostic significance in multiple myeloma datasets, where higher gene expression was associated with poorer survival and faster disease progression, and (ii) elevated expression in myeloma tissue versus NPC from integrated analyses (**Fig. 1B**).

Annotation of SE region to its nearest gene across multiple myeloma cases identified established t(4;14)-specific oncogenes, including *NSD2* and *FGFR3*, serving as a proof of principle of this study. Notably, this selection also included the *HJURP* gene, which has not previously been implicated in multiple myeloma. Significantly high H3K27ac signals were found at the distal and proximal regions near the transcription start sites (TSS) of the *NSD2* and *HJURP* genes in all five t(4;14)-positive HMCLs and the myeloma patient sample (MM 1; **Fig. 1C**). In contrast, only background level signals were present in the control cells, and non–t(4;14)-translocated multiple myeloma patient samples, MM 3 to 10 (Supplementary Fig. S1B). Data of MM 2, another t(4;14)-positive myeloma patient sample, was collected from the study of Jin Y and colleagues, (28) and enrichment of H3K27ac signals was also observed at the enhancer region of *HJURP* gene. The relatively increased enrichment of H3K4me1 to H3K4me3 was observed in H3K27ac-enriched SE region, which was a major epigenomic feature distinguishing enhancers from promoters (29). In addition, we found that there was high enrichment of the H3K4me2 signal at both distal and proximal regions of the *HJURP* gene, which indicated as another epigenetic signature of active enhancers (**Fig. 1D**; ref. 29). Of relevance, the SE lies within the coding region of *TRPM8*, and near to the *SPP2* and *MSL3P1* gene. However, we did not further examine these genes because they do not fulfil the other criteria in our filtering strategy, as illustrated in **Fig. 1B**. These findings indicated that aberrant activation of *HJURP*-SE is specific to t(4;14)-positive multiple myeloma.

We next established the clinical significance of *HJURP* in the development and progression of multiple myeloma, by performing *in silico* analyses on publicly available Gene Expression Omnibus datasets, containing samples from patients with monoclonal gammopathy of undermined significance (MGUS), multiple myeloma, and plasma cell leukemia (**Fig. 1E**). Increased *HJURP* expression level was observed along with multiple myeloma disease progression, with relapsed multiple myeloma cases having the highest expression level. Kaplan–Meier analysis of several myeloma patient (CoMMpass, HOVON, and UAMS) datasets showed high *HJURP* value was associated with a worse overall survival (OS) and progression-free survival (PFS; **Fig. 1F** and **G**; Supplementary Fig. S1C). Therefore, aberrant expression of *HJURP* is of clinical relevance in multiple myeloma.

HJURP gene was aberrantly activated and associated with poor outcomes in multiple myeloma samples with t(4;14) but also those without

We next sought to determine the expression level of *HJURP* in a selected panel of t(4;14) and non-t(4;14) myeloma cell lines. Upregulation of *HJURP* transcript and protein was detected in myeloma cells carrying t(4;14) via qRT-PCR and Western blotting analysis (**Fig. 2A** and **B**). Immunofluorescence (IF) assay further confirmed the increased expression of HJURP in t(4;14)-positive H929 cells compared with the t(4;14)-negative U266 cells (**Fig. 2C**), with the HJURP protein mainly localized to the cellular nucleoplasm & nucleoli (**Fig. 2D**). Analysis of *HJURP* mRNA expression across molecular subtypes of myeloma in the UAMS dataset indicated that there was an evident overexpression of *HJURP* in the t(4;14) subgroup (4p16) compared with the rest ($P = 0.00972$; **Fig. 2E**). However, it is essential to note that high expression of *HJURP* is also observed in other subtypes. This pattern is similarly observed in other datasets (Supplementary Fig. S2A). As the *HJURP* SE was only observed in t(4;14) cell lines and patient samples, we rationalized that generation of the unique SE in 4p16 multiple myeloma cells may be responsible for upregulated *HJURP* expression in t(4;14) myeloma, while other mechanisms may be involved in driving increased expression of *HJURP* in other subtypes of myeloma.

Since *HJURP* expression may be high in both t(4;14) and non-t(4;14) myeloma, and we have earlier shown that high expression of *HJURP* is associated with poorer outcome (**Fig. 1F** and **G**), we further look at the prognostic value of *HJURP* expression in t(4;14) or non-t(4;14) myeloma separately. Higher expression of *HJURP*, either top 25% or higher than the median is associated with poorer survival in both the UAMS and CoMMpass datasets (**Fig. 2F** and **G**; Supplementary Fig. S2B and S2C). Furthermore, multivariate and univariate Cox proportional hazards analyses performed on the UAMS and CoMMpass datasets showed that both elevated *HJURP* and *NSD2* expression were significantly associated with inferior survival, and *HJURP* levels have prognostic value independent of *NSD2* levels for both PFS and OS (Supplementary Table S3). Therefore, *HJURP* overexpression is associated with inferior clinical survival in myeloma, regardless of t(4;14) status.

Genetic inhibition of *HJURP* impaired multiple myeloma cell growth and induced apoptosis

To further interrogate the functional role of *HJURP* in regulating multiple myeloma cell biology, we utilized a loss- and gain-of-function

(*Continued.*) **C,** Immunoblot analysis for apoptotic markers (PARP and cleaved-PARP) in CTRL or shHJURP–transfected KMS28BM and H929 cells. The immunoblot results of HJURP-knockdown in H929 cells were based on the same batch of H929 cell lysates performed at the same time, and the same GAPDH blot was used as a loading control in **A** and **C**. **D,** KMS28BM and H929 cells were transfected with the CTRL or HJURP shRNA vector for 72 hours. Examination for apoptotic was performed by Annexin V staining and flow cytometry. The percentage of apoptotic cells is represented in a bar diagram from three independent experiments. **E,** Representative images of metaphase and anaphase of scramble and shHJURP#2 of H929 cell line. Empty arrowheads, lagging chromosomes; arrowheads, chromosomal bridges; arrows, misaligned metaphase. Scale bars, 10 μm. **F** and **G,** Frequency of anaphase defects, including lagging chromatin, anaphase bridges, or both (**F**) and metaphase defects (e.g., misalignment; **G**) in shHJURP#2 H929 versus scramble. **H,** DAPI (blue) and CENP-A (green) staining in scramble and shHJURP#2 H929 cell line. Quantification was performed in duplicates ($n = 100$ per sample); data are mean ± SEM. Scale bars, 10 μm. **I,** Expression of *HJURP* protein and mRNA were detected upon *HJURP* shRNA transfection or cotransfected with *HJURP* shRNA plus *HJURP* overexpression vector in H929 cell. GAPDH was used as a loading control. **J,** Cell viability was measured in shHJURP–transfected H929 cells, shHJURP–transfected H929 cells stably overexpressing HJURP, or a control shRNA. For each condition, cell viability was measured every 24 hours and compared with day 1. **K,** The percentage of apoptotic cells was measured in shHJURP–transfected H929 cells, shHJURP–transfected H929 cells stably overexpressing *HJURP*, or a control shRNA. Data are presented as mean ± SD of six replicates out of the representative of three independent experiments. Student *t* tests were performed compared with the control. *, $P < 0.05$; **, $P < 0.01$; ***, $P < 0.001$; ****, $P < 0.0001$.

strategy to alter *HJURP* gene expression and then determined its effect on cell growth. Reduction of HJURP expression using short hairpin RNA (shRNA) in KMS28BM and H929 cells (**Fig. 3A**) suppressed multiple myeloma cell growth over 3 days, compared with control shRNA transduced cells (**Fig. 3B**). There is increased apoptosis upon *HJURP* silencing in KMS28BM and H929 (**Fig. 3C** and **D**; Supplementary Fig. S3A). To evaluate the effect of *HJURP* on cell-cycle distribution, DNA content was analyzed by flow cytometry for H929 cells stained with propidium iodide (PI), following mock or *HJURP* shRNA transfection at 72 hours. *HJURP* silencing caused a significant increase in G_1/G_0 populations with a concurrent decrease in S- and G_2–M populations as compared with control treatments (Supplementary Fig. S3B). *HJURP* was previously reported as a major CENP-A chaperone, which has played a crucial role in the CENP-A loading at the centromeres (30, 31). Consistently with previous reports, chromosome segregation defects including lagging chromosomes, chromosomal bridges, and metaphase defects were detected in *HJURP*-deficient myeloma cells (**Fig. 3E–G**). From the immunostaining analysis, the centromeric association of CENP-A was lost in cells depleted of HJURP (**Fig. 3H**).

Next, we performed rescue experiments by exogenously overexpressing HJURP in H929 cells that had been stably transduced with *HJURP* shRNA. We first confirmed a successful *HJURP* protein and mRNA restoration in this setting (**Fig. 3I**). Rescue of the *HJURP* knockdown H929 cell lines with *HJURP* overexpression improved cell growth (**Fig. 3J**), and reduced apoptosis (**Fig. 3K**; Supplementary Fig. S3C). Additionally, we observed that *HJURP* overexpression in the non-t(4;14) RPMI-8226 cell promoted cell growth (Supplementary Fig. S3D and S3E), with reduction in apoptosis and an increase in S-phase populations (Supplementary Fig. S3F and S3G). These findings collectively suggested that overexpression of *HJURP* promoted cell growth and suppressed cell apoptosis in both t(4;14) and non-t(4;4) myeloma, and is functionally relevant in myeloma.

Repression of SE activity inhibited *HJURP* transcription and phenocopied *HJURP* silencing

SEs function depends on the binding of transcriptional factors and coactivators, including CDK7 and bromodomain and extra-terminal (BET) bromodomains, to drive downstream gene transcription (13, 14). We next investigated the effect of SE activity on *HJURP* transcription. t(4;14)-positive H929 and KMS28BM cells were treated with a specific inhibitor targeting CDK7 (THZ1), as a chemical tool to help identify potentially relevant and functional SE-associated genes. Downregulation of *HJURP* upon THZ1 treatment was confirmed by qRT-PCR and immunoblot in a dose-dependent manner (**Fig. 4A** and **B**). Similarly, JQ1, a small-molecule inhibitor blocking BRD4 binding to SE regions, also diminished the mRNA levels of *HJURP* (Supplementary Fig. S4A). As t(4:14)-negative cells show no prominent SE activity and *HJURP* overexpression, when RPMI8226 and U266 were treated with THZ1 or JQ1 for 24 hours, we observed no significant decreased *HJURP* expression as expected (Supplementary Fig. S4B). In addition, THZ1 produced a potent antiproliferative effect associated with cell-cycle arrest and increased cellular apoptosis of myeloma cells (Supplementary Fig. S4C–S4G). Together, these results indicated that *HJURP* expression was sensitive to transcriptional inhibition, a general characteristic of SE-driven genes.

We then employed CRISPR interference (CRISPRi), in which three single-guide RNAs (sgRNA) were designed to target multiple sites of the SE region, to recruit the dCas9-KRAB and interfere with the SE-promoter interaction (**Fig. 4C**). After confirming the change of *HJURP* expression at the mRNA levels in sgHJURP-transfected myeloma cells, two effective sgRNAs (sgHJURP #1 and sgHJURP #2) were selected for subsequent functional assay (Supplementary Fig. S4H). Blockade of two effective individual constituent sites within SE region reduced *HJURP* protein and mRNA expression levels (**Fig. 4D** and **E**), showing that SE could positively regulate *HJURP* transcription. As expected, we observed that enrichment of H3K27ac signals, indicative of active enhancers, were reduced at the SE region of *HJURP* locus upon CRISPRi-mediated suppression (Supplementary Fig. S4I). Furthermore, the inhibition of SE activity in SE-CRISPR/dCas9-transfected cells led to a significant decrease in cell survival (**Fig. 4F**). The CRISPR interference-SE group also showed a higher apoptosis rate than the control group in KMS28BM and H929 cells (**Fig. 4G**; Supplementary Fig. S4J). We also observed that expression of several key apoptosis markers such as cleaved PARP, cleaved caspase-3, cleaved caspase-9, and cleaved caspase-7 were increased upon CRISPR interference of SE function, compared with the control group (**Fig. 4H**; Supplementary Fig. S4K). These findings supported SE-mediated epigenetic control as the primary driver for *HJURP* activation in t(4;14) multiple myeloma and is important for the downstream functional effect of *HJURP*.

Remote SE interacted with *HJURP* promoter and facilitated gene transcription

Our ChIP-seq analysis demonstrated that *HJURP*-SE was located around 120 kb to the TSS of *HJURP* gene. Hence, we then investigated the potential long-range interaction between the distal SE and promoter elements. The binding profile for H3K27ac identified four peaks (E1–E4) within *HJURP*-SE in H929 cells (**Fig. 5A**). Of the four constituent enhancers, the active E2 element was associated with the highest H3K27ac signals (**Fig. 5B**). We found that THZ1 suppresses the H3K27ac mark on chromatin (**Fig. 5C**). The ability of SE to regulate the transcriptional activities of the *HJURP* promoters was tested by luciferase reporter assay. Two loci within SE region (named pGL3–1.1 and pGL3–1.2) and a negative control locus named pGL3-basic outside these fragments were amplified and cloned into upstream of the pGL3-enhancer constructs. pGL3–1.1 related to the E1 and E2, and the start position and end position was chr2: 234,873,330–234,875,324. The pGL3–1.2 related to the E3 and E4, and the start and end position was chr2:234,875,382–234,878,373. The sequences of SE fragments inserted into each vector were presented in Supplementary Table S4. We observed that the enhancer (pGL3–1.1 and pGL3–1.2) group showed significantly increased luciferase activity compared with the corresponding control (**Fig. 5D**).

4C allows the unbiased detection of all genomic regions that physically interact with a particular region of interest (25). We explored the potential long-range interaction between SE and *HJURP* gene promoter using 4C sequencing (4C-seq) analyses, following THZ1 treatment (50 nmol/L, 24 hours). We designed one PCR primer near SE element (viewpoint). Then we calculated each interaction and showed a heatmap comparing THZ1 (experiment) with DMSO (control). From the visualization of the result output, we observed a decrease in chromatin–chromatin interaction near the *HJURP* promoter, amongst other enhancer-promoter interactions affected (**Fig. 5E**). Collectively, these findings indicated that SE could drive *HJURP* transcription via potential long-range interaction between the distal SE and promoter elements.

NSD2 promoted *HJURP* gene transcription

The histone lysine methyltransferase *NSD2* (also named *MMSET* or *WHSC1*) is overexpressed in myeloma cases due to the t(4;14) chromosomal translocation (32). *NSD2* catalyzes dimethylation of lysine

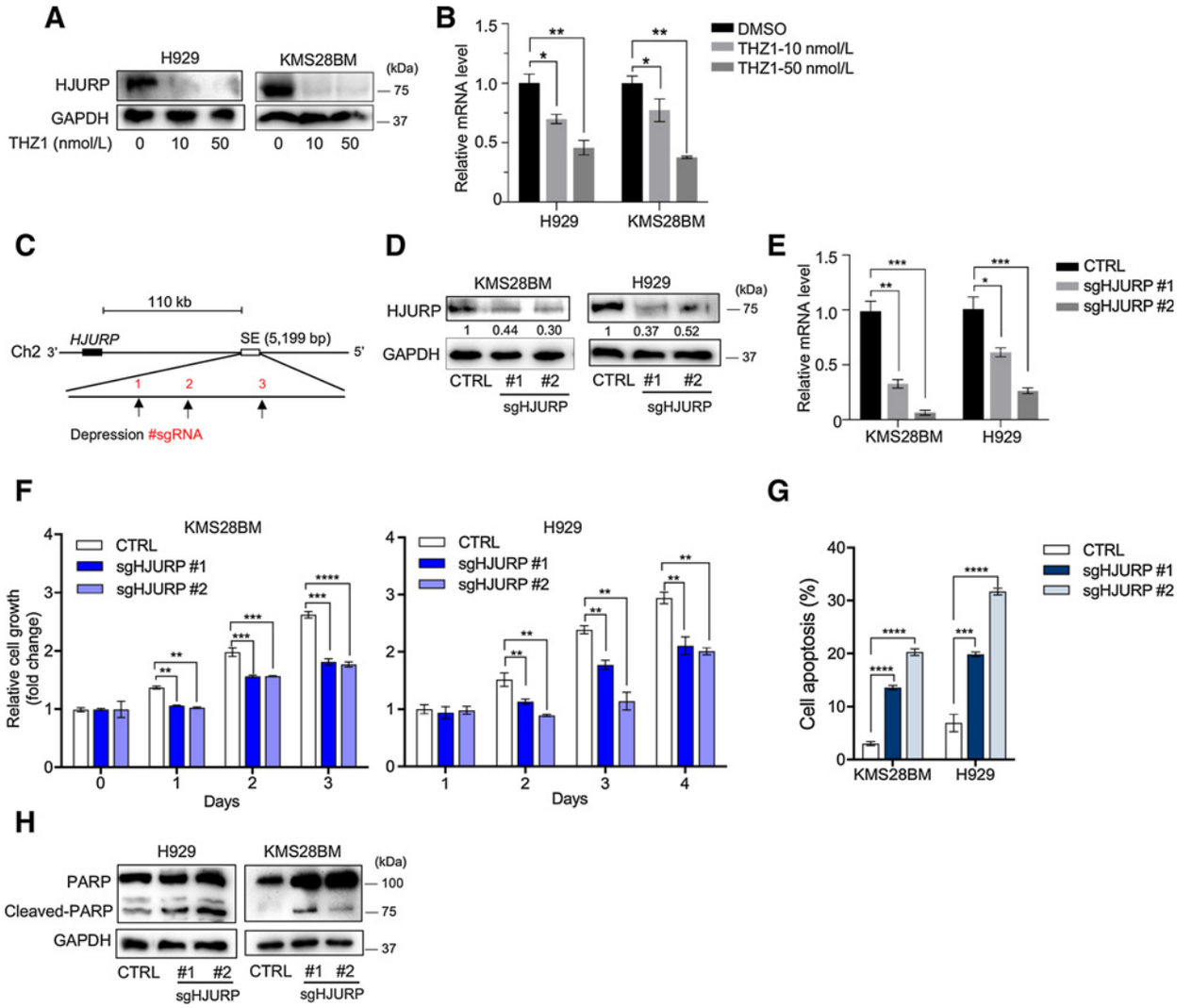

Figure 4.

Genomic editing to disrupt SE region repressed *HJURP* transcription and mimicked phenotypic effects of *HJURP* silencing. **A** and **B,** H929 and KMS28BM cells were treated with DMSO or THZ1 at a concentration of 10 nmol/L and 50 nmol/L for 24 hours, and *HJURP* expression level was analyzed by Western blotting (**A**) and qRT-PCR (**B**). GAPDH was used as a loading control. **C,** A schematic diagram of the sgRNA-directed dCas9-KRAB transcription repression system and three sgRNAs designed to target multiple sites of the SE region of *HJURP*. CRISPR-based gene editing of indicated SE region repressing gene transcription. **D** and **E,** Protein expression (**D**) and mRNA (**E**) levels of *HJURP* in KMS28BM and H929 cells upon depression of SE activity by two individual sgRNAs (sgHJURP#1 and sgHJURP#2) or transfected with the control vector (CTRL). **F,** Depression of *HJURP* SE region abrogated cell viability in KMS28BM and H929 cells. **G,** Cell apoptosis was determined 72 hours after depression of HJURP-SE in KMS28BM and H929 cells. Cells were stained with Annexin V and PI and analyzed by flow cytometer. **H,** PARP cleavage was analyzed by Western blot in KMS28BM and H929 cells mock infected or infected with sgHJURP#1 and sgHJURP#2 for 72 hours. Detection of GAPDH protein was used as an internal loading control. Data are presented as mean ± SD of six replicates out of the representative of three independent experiments. Student *t* tests were performed compared with the control. *, $P < 0.05$; **, $P < 0.01$; ***, $P < 0.001$; ****, $P < 0.0001$ by two-sample.

36 on histone H3 (H3K36me2), and *NSD2* overexpression leads to a global increase in this modification, accompanied by a concomitant global decrease in repressive marker H3K27me3 methylation. The genomic disorganization generated by *NSD2* created a disarrayed genomic landscape that is sufficient for activating target genes and initiating oncogenic programming (33).

To study whether *NSD2* could regulate *HJURP* transcription in t(4;14)-positive cells, we first knocked down *NSD2* using two independent shRNAs. This resulted in a significant decrease in *HJURP* protein and mRNA expression (**Fig. 6A** and **B**; Supplementary Fig. S5A), indicating that *HJURP* could be a downstream target gene of *NSD2*. To further verify this, we utilized an established isogenic pair of KMS11 cell lines, where *NSD2* was either deleted by knocking out the translocated overexpressed allele ($KMS11^{TKO}$; NSD2-low) or the wild-type (WT) nontranslocated allele ($KMS11^{PAR}$; NSD2-high; ref. 34). As expected, *NSD2* knockout in $KMS11^{TKO}$ cell led to the loss of *HJURP* expression, while *NSD2* overexpression-transfected $KMS11^{TKO}$ cell presented reincreased *HJURP* expression (**Fig. 6C** and **D**). We next assessed the effect of *NSD2* on *HJURP* expression in t(4:14)-negative myeloma cells. Similar to myeloma cell carrying

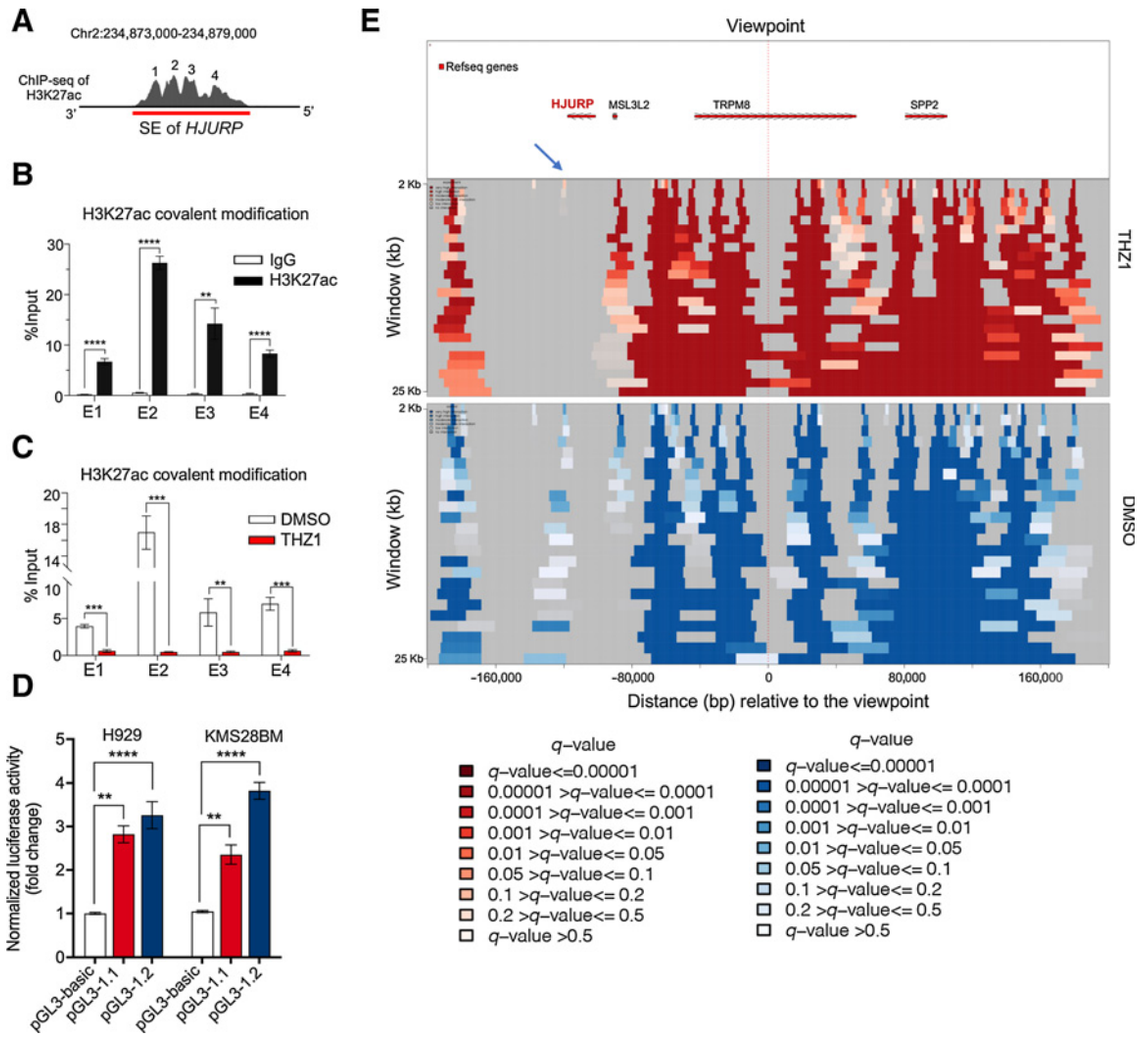

Figure 5.

Remote SE interacted with the *HJURP* promoter and facilitated gene transcription. **A,** The binding profile for H3K27ac identified four peaks (E1–E4) within *HJURP*-SE in H929 cells. E1, E2, E3, and E4 schematic of SE region and positions of primer sets used for ChIP-qPCR. **B,** ChIP-qPCR analysis of H3K27ac binding at constituent enhancers (E1–E4) in H929 cells. The anti-IgG was used as the negative control. Of the four constituent enhancers, the active E2 element was associated with the highest H3K27ac signals. **C,** ChIP-qPCR analysis of H3K27ac binding at constituent enhancers (E1–E4) within SE region in DMSO/THZ1-treated H929 cells. H3K27ac recruitment to the chromatin of *HJURP*-SE was suppressed upon THZ1 treatment (50 nmol/L; 24 hours). **D,** Separate fragments of SE regions (named pGL3–1.1 and pGL3–1.2), which were subcloned upstream of the luciferase reporter gene. Dual luciferase reporter assays examining SE activities 72 hours posttransfection in KMS28BM and H929 cells. Firefly luciferase activity was measured and normalized to *Renilla* luciferase to control cell number and transfection efficiency and is expressed as a ratio relative to activity of the control enhancer construct. **E,** 4C-seq experiments were performed to unbiasedly detect all genomic regions that interact with the indicated SE. Genomic DNA samples of H929 cells were harvested upon THZ1 (top) or DMSO (bottom) treatment for 24 hours and subjected to a 4C assay. The top track presents 4C-seq data for the viewpoint (SE), marked by a vertical highlight in each panel. Color codes represent the quantitative scale (*q*-value). Blue arrowhead, *HJURP* promoter. Data are presented as mean ± SD of six replicates out of the representative of three independent experiments. *P* values were derived from *t* tests. **, $P < 0.01$; ***, $P < 0.001$; ****, $P < 0.0001$ by two-sample.

t(4;14), *NSD2* overexpression caused elevated *HJURP* expression as well as increased abundance of H3K27ac at the *HJURP* promoter and SE region (Supplementary Fig. S5B and S5C). These results indicated that *NSD2* as a key regulator contributing to elevated expressions of *HJURP* with upregulated H3K27ac signal in the *HJURP* promoter and enhancer regions.

Furthermore, the presence of *NSD2* increased H3K36me2 abundance towards H3K27ac-containing chromatin of *HJURP* SE, with decreased enrichment of H3K27me3 in t(4;14)-positive myeloma cell (**Fig. 6E**; Supplementary Fig. S5D). Early reports demonstrated that *NSD2* overexpression leads to genome-wide spreading of H3K36me2 from active gene bodies into intergenic regions, which provides a favorable environment for H3K27ac binding linked to oncogene activation (35). Here we hypothesized that transcriptional activation of *HJURP* could partially be dependent on NSD2-mediated global alteration of histone modification in t(4;14)-positive myeloma cells. Together, these data argued for a model in which t(4;14)-driven *NSD2* overexpression leads to a permissive genome-wide epigenetic environment for aberrant enrichment of H3K36me2 and H3K27ac at normally silent cancer-associated genes (*HJURP* being a specific example), triggering increased expression of these genes.

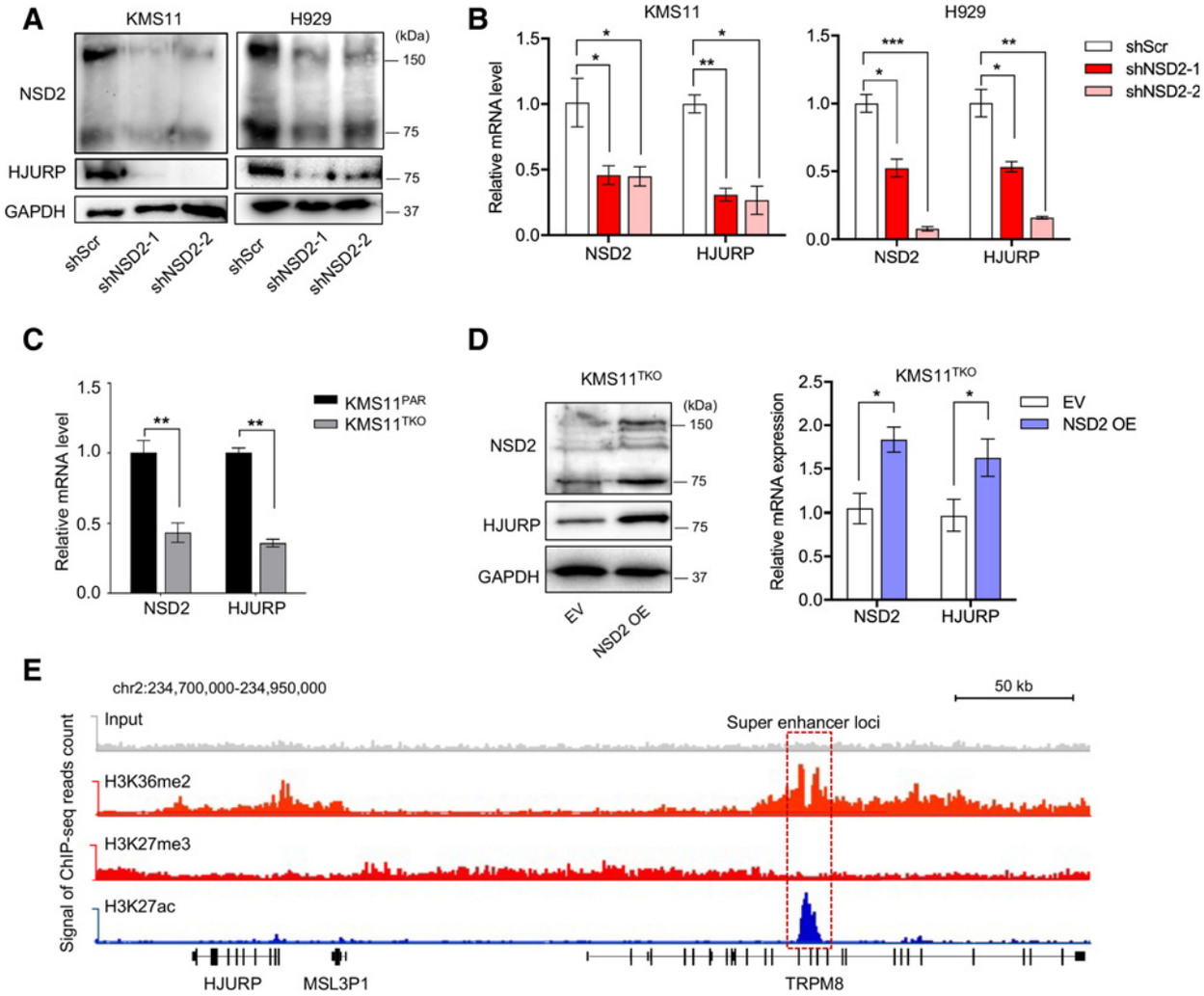

Figure 6.

NSD2 positively regulated *HJURP* transcription. **A** and **B,** The protein (**A**) and mRNA (**B**) expression levels of *HJURP* and *NSD2* were detected by qRT-PCR and Western blot upon transfection with two different pairs of *NSD2* shRNA (shNSD2–1 and shNSD2–2) or the negative control shRNA (shScr) in KMS11 and H929 cells. GAPDH was measured as the loading control and was used for data normalization. **C,** mRNA expression levels of *NSD2* and *HJURP* were detected by qRT-PCR analysis in KMS11^{PAR} and KMS11^{TKO} cells. **D,** Western blot and qRT-PCR analysis demonstrated that the overexpression of *NSD2* increased *HJURP* gene transcription in KMS11^{TKO} cell. **E,** ChIP-seq data tracks showing the abundance of H3K36me2, H3K27me3, and H3K27ac within *HJURP* loci and its SE region of H929 cells. Public H3K36me2 and H3K27me3 ChIP-seq data were collected and visualized by the ChIP-Atlas database (https://chip-atlas.org/). Data are presented as mean ± SD of six replicates out of the representative of three independent experiments. *P* values were derived from *t* tests. *, $P < 0.05$; **, $P < 0.01$; ***, $P < 0.001$ by two-sample.

NSD2 interacted with *BRD4* to facilitate *HJURP*-SE activation

Next, we determined the chromatin state at the *HJURP* SE and how *NSD2* regulated *HJURP* gene transcription. Luciferase reporter assays were performed in t(4;14)-positive myeloma cells to functionally test the effect of *NSD2* on the SE and HJURP-promoter activity. We observed the activity of *HJURP* promoter-luciferase reporter in KMS11 cells cotransfected with NSD2-overexpressed vector was increased by approximately eight-fold. In addition, cotransfection of *NSD2*-overexpressed vector with SE-driven luciferase plasmid vector (pGL3–1.1 and pGL3–1.2) increased luciferase activity by approximately four-fold (**Fig. 7A**). Similar patterns of luciferase reporter activities were also detected in the H929 and KMS28BM cells (**Fig. 7A**; Supplementary Fig. S6A). The sequence of SE fragments inserted into luciferase plasmid vector was presented in Supplementary Table S4.

Because *NSD2* does not contain a DNA-binding domain, it cannot bind directly to a gene promoter or enhancer to regulate gene transcription. To investigate how *NSD2* activated *HJURP* gene expression, we performed the stable isotope labelling by amino acids in cell culture (SILAC)-based in conjunction with mass spectrometry analysis to determine *NSD2*-interacting proteins. Interestingly, *BRD4* was identified as one potential *NSD2*-interacting protein in KMS11 cells (Supplementary Table S5). The bromodomain protein BRD4 was previously reported as an *NSD2*-interacting protein, which was required for transcription elongation and enhancer activation (36). Here, we found that *BRD4* was coimmunoprecipitated with *NSD2* protein and vice versa (**Fig. 7B**), in agreement with a recent study of the interaction between *NSD2* and *BRD4* in pluripotent stem cells (37).

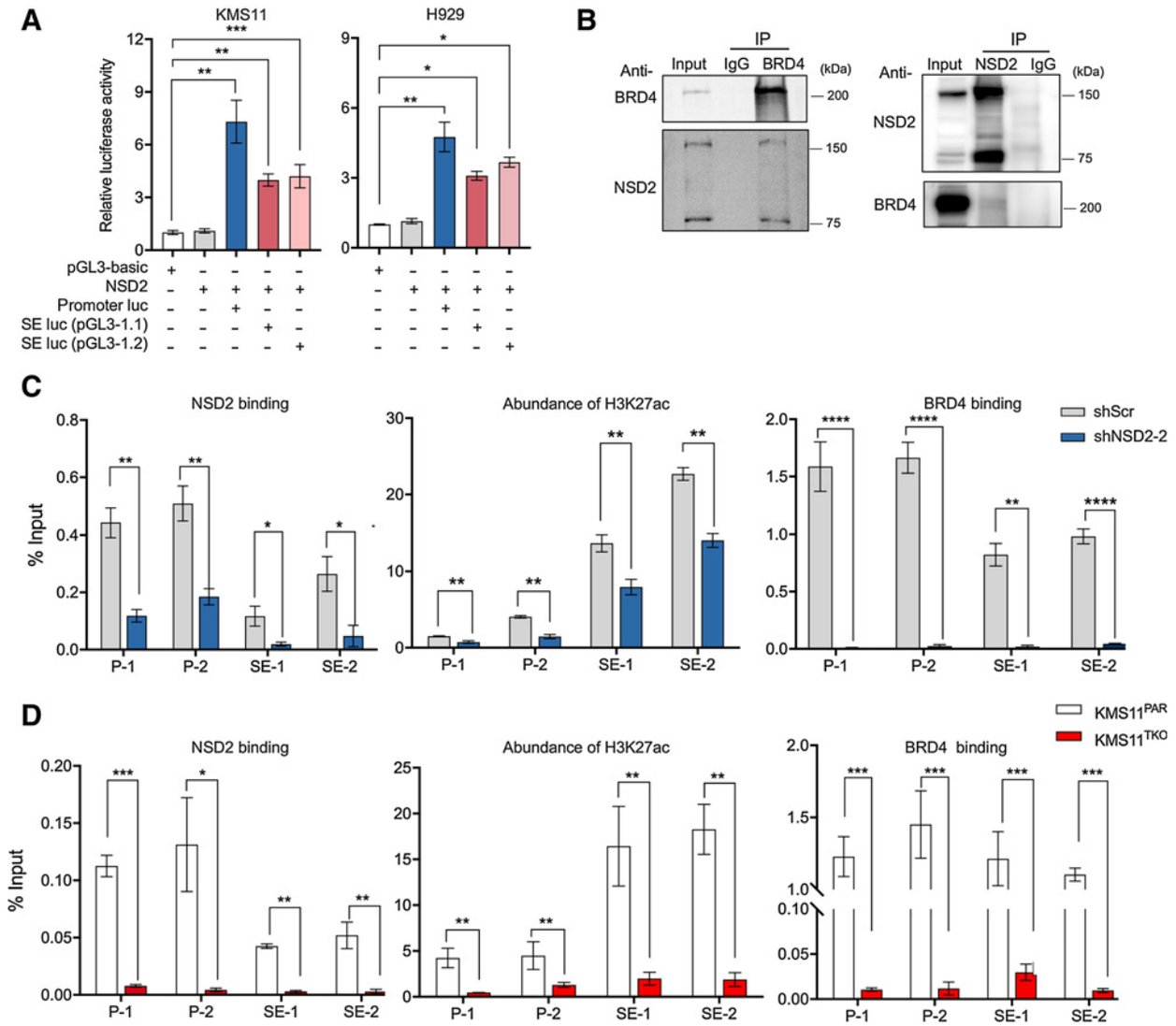

Figure 7.

NSD2 interacted with *BRD4* to facilitate activation of *HJURP* super enhancer. **A,** Luciferase assay analysis of transcription activation in H929 and KMS11 cells transfected with pGL3-basic (control) alone, *HJURP*-promoter luciferase vectors alone, SE luciferase reporter vectors alone (pGL3–1.1 and pGL3–1.2), or co-transfected with NSD2 overexpression vector. **B,** Reciprocal coimmunoprecipitation of endogenous BRD4 and NSD2 in KMS11 cells. **C,** NSD2, BRD4 binding ability, and abundance of H3K27ac were measured at the promoter and SE region in CON/NSD2-knockdown H929 cells. Silencing of NSD2 reduced the recruitment of H3K27ac, BRD4 as well as NSD2 itself to the promoter and SE region of *HJURP*. **D,** NSD2, BRD4 binding ability, and abundance of H3K27ac at the promoter and SE region of *HJURP* in KMS11^{PAR} and KMS11^{TKO} cells. Data are presented as mean ± SD of six replicates out of the representative of three independent experiments. *P* values were derived from *t* tests. *, $P < 0.05$; **, $P < 0.01$; ***, $P < 0.001$; ****, $P < 0.0001$ by two-sample.

We then accessed the recruitment of *NSD2*, H3K27ac, and BRD4 proteins to the promoter and SE region of the *HJURP* gene. Silencing of NSD2 in H929 cells reduced the abundance of H3K27ac, and the recruitment of BRD4 as well as NSD2 itself to the promoter (indicated as P-1 and P-2) and SE region (indicated as SE-1 and SE-2), suggesting that *NSD2* may function as a scaffold to recruit H3K27ac and BRD4, which promoted *HJURP* transcription (**Fig. 7C**; Supplementary Fig. S6B). Consistently, suppression of H3K27ac, BRD4, and *NSD2* binding to *HJURP* promoter and SE were also observed in KMS11^{TKO} cells when compared to the WT KMS11^{PAR} cells (**Fig. 7D**). Previous reports proposed that BRD4 plays an essential role in *NSD2* recruitment to chromatin (37). We treated H929 cells with DMSO or JQ1 for 24 hours, and checked *NSD2* binding affinity to *HJURP* promoter and SE chromatin. Suppression of BRD4 has a limited effect on *NSD2* binding affinity to the *HJURP* promoter and SE (Supplementary Fig. S6C). These results suggested that the recruitment of *NSD2* to chromatin in the t(4;14) myeloma cell lines may be independent of BRD4. Given the evidence presented for a role of *NSD2* in regulating *HJURP* gene transcription and the physical association between *NSD2* and *BRD4*, the NSD2/BRD4 complex is anticipated to be recruited to the *HJURP* gene promoter and SE, and may cooperatively facilitate gene transcription elongation (Supplementary Fig. S6D).

Discussion

SEs are groups of enhancers in close genomic proximity with aberrant high levels of transcription factors binding, which are central to driving gene expression in controlling cell identity and stimulating oncogenic transcription. In an effort to search for novel oncogenic drivers and potential therapeutic targets, we utilized a transcriptional CDK7 inhibitor, THZ1, coupled with H3K27ac ChIP-seq and transcriptome analyses, to identify novel SE-associated genes of functional relevance. Using this strategy, we identified the holiday junction recognition protein (*HJURP*) as a novel SE-driven transcript of t(4;14)-positive multiple myeloma. Elevated *HJURP* was associated with myeloma disease progression and poor patients' outcomes. Experimentally, overexpression of *HJURP* mediated increased cell growth and protection from apoptosis in myeloma cells. Mechanistically, we demonstrated that the SE observed uniquely in t(4;14) myeloma interacted with *HJURP* promoter, and the NSD2/BRD4 complex was recruited to the promoter and SE region of *HJURP* gene, thus facilitating *HJURP* gene transcription.

The oncogenic function of *HJURP* has been reported in the progression of lung cancer, breast cancer, brain cancer, liver cancer, and ovary cancer (38–43) and elevation of *HJURP* is also strongly correlated with unfavorable prognosis of patients with cancer (44, 45). The histone chaperone *HJURP* is a chromatin assembly factor for CENP-A nucleosomes deposition and maintenance at centromeres (30, 31). *HJURP* functioned as a repressor for deregulation of recombination in the rDNA region and maintained chromosomal stability, resulting in cancer cell immortalization (38). In bladder cancer, *HJURP* regulated cell proliferation and apoptosis via PPARγ-SIRT1 negative feedback loop (40). Compared with normal plasma cells and also other genetic subtypes of myeloma, we found that the aberrant SE formation downstream TSS of *HJURP* gene found specifically in t(4;14) myeloma, interacted with *HJURP* promoter and resulted in its increased expression. Of note, we observed *HJURP* overexpression in non-t(4;14) myeloma and associated with poor outcomes. Other mechanisms may therefore be involved in driving *HJURP* expression in the non-t(4;14) myeloma and will require further studies to elucidate. Of note, *HJURP* expression correlated with poor prognosis in multiple myeloma. These high-risk patients with multiple myeloma may benefit from personalized treatment strategies that target underlying molecular mechanisms.

NSD2 activity influences myelomagenesis, and *NSD2* overexpression is universal with t(4;14) translocation (6). In t(4;14)- positive myeloma, loss of *NSD2* inhibited cell growth, caused cell-cycle arrest, induced apoptosis, and alteration of cell adhesion (7,8), Early studies demonstrated that *NSD2* reprogramed histone methylation and modulated chromatin remodeling, and led to a global upregulation of target gene transcription (33, 34). More recently, overexpression of *NSD2* was revealed to leads to alteration in H3K27ac enrichment, a mark that is associated with active enhancers and promoters and to drive oncogenic transcriptional programs (35). Enhancer activation requires the presence of specific recognition sequences for the cooperative recruitment of DNA-binding transcription factors and their cofactors that initially activate gene expression. *NSD2* is a H3K36 methyl transferase, and *NSD2* overexpressed deposits the chromatin mark at an increased rate with a global increase in H3K36me2, and thus new enhancer regions become available. As exemplified by our study demonstrating the activation of SE-driven *HJURP* transcription, we suggest that *NSD2* may alter H3K27ac enrichment and make the *HJURP* SE regions available in t(4;14) myeloma cells.

The role of *NSD2* has been linked to transcriptional elongation through interactions with BRD4, pTEFb, and HIRA (46). BRD4 mediated the recruitment of *NSD2* to the TSS of certain genes. In acute myeloid leukemia, a short isoform of NSD3 (another member of the NSD family), lacking the SET domain, can act together with BRD4 on enhancers-related genes that contribute to disease progression (47). In tamoxifen-resistant breast cancer, *NSD2* was recruited to the *ERα* gene by the epigenomic proteins BRD3/4, and are essential regulators of estrogen receptor signaling (48). Our findings showed that *NSD2* is important for binding of BRD4 and the abundance of H3K27ac to the active parts of SE and promoter chromatin, and the NSD2-BRD4 complex plays a role in activating *HJURP* expression. Actually, the recruitment and binding of *NSD2* to these regions are independent of BRD4. It will be interesting to elucidate whether the function of *NSD2* described here is also involved in other *NSD2* target genes regulation in t(4;14)-positive multiple myeloma. Our study collectively identified *HJURP* as a novel SE-associated gene in myeloma, that promotes growth and survival. In t(4;14) myeloma, it is regulated through a novel SE uniquely present in this subtype of multiple myeloma, which is a downstream target of *NSD2*. This transcriptional regulation requires chromatin interaction and binding of *NSD2 and BRD4* to the SE associated with *HJURP*. SE-driven *HJURP* could be a novel therapeutic target for t(4;14)-translocated multiple myeloma.

Authors' Disclosures

T. Sanda reports grants from National Medical Research Council during the conduct of the study. M.J. Fullwood reports a patent for ChIA-PET method issued and a patent for updated ChIA-PET method issued. No disclosures were reported by the other authors.

Authors' Contributions

Y. Jia: Conceptualization, investigation, visualization, writing–original draft, writing–review and editing. **J. Zhou:** Data curation, formal analysis, supervision, writing–review and editing. **T.K. Tan:** Data curation, investigation, visualization, methodology. **T.-H. Chung:** Validation, investigation, methodology. **Y. Chen:** Validation, investigation, methodology. **J.-Y. Chooi:** Methodology. **T. Sanda:** Resources, writing–review and editing. **M.J. Fullwood:** Formal analysis, methodology, writing–review and editing. **S. Xiong:** Investigation. **S.H.M. Toh:** Investigation. **K. Balan:** Validation. **R.W.J. Wong:** Formal analysis, writing–review and editing. **J.S.L. Lim:** Validation, investigation. **E. Zhang:** Resources, investigation. **Z. Cai:** Resources, investigation. **P. Shen:** Writing–review and editing. **W.J. Chng:** Conceptualization, resources, formal analysis, supervision, funding acquisition, writing–original draft, writing–review and editing.

Acknowledgments

The work was supported by the National Research Foundation Singapore and the Singapore Ministry of Education under its Research Centres of Excellence initiative (to W.J. Chng), the NMRC Clinician Scientist Investigator award (to W.J. Chng), the RNA Biology Center at CSI Singapore, NUS, from funding by the Singapore Ministry of Education's Tier 3 grants, grant number MOE2014-T3–1-006 (to W.J. Chng), the National Natural Science Foundation of China (grant no. 82000212 to Y. Jia), Natural Science Foundation of Zhejiang Province (grant no. LQ21H160022 to Y. Jia), Medical Health Science and Technology Project of Zhejiang Provincial Health Commission (grant no. 2021RC003 to Y. Jia).

Y. Jia also thanks the China Scholarship Council (grant no. 201706320167) for financial support to visit National University of Singapore. The authors thank Mr. Victor Chua Kai Chuan for his assistance in IF experiments.

The costs of publication of this article were defrayed in part by the payment of page charges. This article must therefore be hereby marked *advertisement* in accordance with 18 U.S.C. Section 1734 solely to indicate this fact.

Received March 25, 2021; revised October 5, 2021; accepted November 30, 2021; published first December 10, 2021.

References

1. Kumar SK, Rajkumar V, Kyle RA, van Duin M, Sonneveld P, Mateos MV, et al. Multiple myeloma. Nat Rev Dis Primers 2017;3:17046.
2. Morgan GJ, Walker BA, Davies FE. The genetic architecture of multiple myeloma. Nat Rev Cancer 2012;12:335.
3. Bergsagel PL, Kuehl WM. Chromosome translocations in multiple myeloma. Oncogene 2001;20:5611–22.
4. Bergsagel PL, Chesi M, Nardini E, Brents LA, Kirby SL, Kuehl WM. Promiscuous translocations into immunoglobulin heavy chain switch regions in multiple myeloma. Proc Natl Acad Sci U S A 1996;93:13931–6.
5. Nishida K, Tamura A, Nakazawa N, Ueda Y, Abe T, Matsuda F, et al. The Ig heavy chain gene is frequently involved in chromosomal translocations in multiple myeloma and plasma cell leukemia as detected by in situ hybridization. Blood 1997;90:526–34.
6. Chesi M, Nardini E, Lim RS, Smith KD, Kuehl WM, Bergsagel PL. The t(4; 14) translocation in myeloma dysregulates both FGFR3 and a novel gene, MMSET, resulting in IgH/MMSET hybrid transcripts. Blood 1998;92:3025–34.
7. Lauring J, Abukhdeir AM, Konishi H, Garay JP, Gustin JP, Wang Q, et al. The multiple myeloma–associated MMSET gene contributes to cellular adhesion, clonogenic growth, and tumorigenicity. Blood 2008;111:856–64.
8. Keats JJ, Reiman T, Maxwell CA, Taylor BJ, Larratt LM, Mant MJ, et al. In multiple myeloma, t(4; 14)(p16; q32) is an adverse prognostic factor irrespective of FGFR3 expression. Blood 2003;101:1520–9.
9. Bradner JE, Hnisz D, Young RA. Transcriptional addiction in cancer. Cell 2017; 168:629–43.
10. Ell B, Kang Y. Transcriptional control of cancer metastasis. Trends Cell Biol 2013;23:603–11.
11. Hnisz D, Abraham BJ, Lee TI, Lau A, Saint-André V, Sigova AA, et al. Super-enhancers in the control of cell identity and disease. Cell 2013;155:934–47.
12. Whyte WA, Orlando DA, Hnisz D, Abraham BJ, Lin CY, Kagey MH, et al. Master transcription factors and mediator establish super-enhancers at key cell identity genes. Cell 2013;153:307–19.
13. Pott S, Lieb JD. What are super-enhancers?. Nat Genet 2015;47:8–12.
14. Hnisz D, Abraham B, Lee T, Lau A, Saint-Andre V, Sigova A, et al. Transcriptional super-enhancers connected to cell identity and disease. Cell 2013;155: 934–47.
15. Chapuy B, McKeown MR, Lin CY, Monti S, Roemer MG, Qi J, et al. Discovery and characterization of super-enhancer-associated dependencies in diffuse large B cell lymphoma. Cancer Cell 2013;24:777–90.
16. Hnisz D, Schuijers J, Lin CY, Weintraub AS, Abraham BJ, Lee TI, et al. Convergence of developmental and oncogenic signaling pathways at transcriptional super-enhancers. Mol Cell 2015;58:362–70.
17. Jia Y, Chng WJ, Zhou J. Super-enhancers: critical roles and therapeutic targets in hematologic malignancies. J Hematol Oncol 2019;12:77.
18. Kwiatkowski N, Zhang T, Rahl PB, Abraham BJ, Reddy J, Ficarro SB, et al. Targeting transcription regulation in cancer with a covalent CDK7 inhibitor. Nature 2014;511:616–20.
19. Wang Y, Zhang T, Kwiatkowski N, Abraham BJ, Lee TI, Xie S, et al. CDK7-dependent transcriptional addiction in triple-negative breast cancer. Cell 2015; 163:174–86.
20. Cheng ZJ, Miao DL, Su QY, Tang XL, Wang XL, Deng LB, et al. THZ1 suppresses human non-small-cell lung cancer cells in vitro through interference with cancer metabolism. Acta Pharmacol Sin 2019;40:814–22.
21. Chipumuro E, Marco E, Christensen CL, Kwiatkowski N, Zhang T, Hatheway CM, et al. CDK7 inhibition suppresses super-enhancer-linked oncogenic transcription in MYCN-driven cancer. Cell 2014;159:1126–39.
22. Jiang YY, Lin DC, Mayakonda A, Hazawa M, Ding LW, Chien WW, et al. Targeting super-enhancer-associated oncogenes in oesophageal squamous cell carcinoma. Gut 2017;66:1358–68.
23. Wong RW, Ngoc PC, Leong WZ, Yam AW, Zhang T, Asamitsu K, et al. Enhancer profiling identifies critical cancer genes and characterizes cell identity in adult T-cell leukemia. Blood 2017;130:2326–38.
24. Jia Y, Zhou J, Tan TK, Chung TH, Wong RWJ, Chooi JY, et al. Myeloma-specific superenhancers affect genes of biological and clinical relevance in myeloma. Blood Cancer J 2021;11:32.
25. van de Werken HJG, de Vree PJP, Splinter E, Holwerda SJB, Klous P, de Wit E, et al. 4C technology: protocols and data analysis. Methods Enzymol 2012;513: 89–112.
26. Mifsud B, Tavares-Cadete F, Young AN, Sugar R, Schoenfelder S, Ferreira L, et al. Mapping long-range promoter contacts in human cells with high-resolution capture Hi-C. Nat Genet 2015;47:598–606.
27. Matsui Y, Nakayama Y, Okamoto M, Fukumoto Y, Yamaguchi N. Enrichment of cell populations in metaphase, anaphase, and telophase by synchronization using nocodazole and blebbistatin: a novel method suitable for examining dynamic changes in proteins during mitotic progression. Eur J Cell Biol 2012;91:413–9.
28. Jin Y, Chen K, De Paepe A, Hellqvist E, Krstic AD, Metang L, et al. Active enhancer and chromatin accessibility landscapes chart the regulatory network of primary multiple myeloma. Blood 2018;131:2138–50.
29. Pekowska A, Benoukraf T, Zacarias-Cabeza J, Belhocine M, Koch F, Holota H, et al. H3K4 tri-methylation provides an epigenetic signature of active enhancers. EMBO J 2011;30:4198–210.
30. Foltz DR, Jansen LE, Bailey AO, Yates JR III, Bassett EA, Wood S, et al. Centromere-specific assembly of CENP-a nucleosomes is mediated by HJURP. Cell 2009;137:472–84.
31. Dunleavy EM, Roche D, Tagami H, Lacoste N, Ray-Gallet D, Nakamura Y, et al. HJURP is a cell-cycle-dependent maintenance and deposition factor of CENP-A at centromeres. Cell 2009;137:485–97.
32. Mirabella F, Wu P, Wardell CP, Kaiser MF, Walker BA, Johnson DC, et al. MMSET is the key molecular target in t (4; 14) myeloma. Blood Cancer 2013;3: e114.
33. Martinez-Garcia E, Popovic R, Min DJ, Sweet SM, Thomas PM, Zamdborg L, et al. The MMSET histone methyl transferase switches global histone methylation and alters gene expression in t (4; 14) multiple myeloma cells. Blood 2011; 117:211–20.
34. Kuo AJ, Cheung P, Chen K, Zee BM, Kioi M, Lauring J, et al. NSD2 links dimethylation of histone H3 at lysine 36 to oncogenic programming. Mol Cell 2011;44:609–20.
35. Lhoumaud P, Badri S, Rodriguez-Hernaez J, Sakellaropoulos T, Sethia G, Kloetgen A, et al. NSD2 overexpression drives clustered chromatin and transcriptional changes in a subset of insulated domains. Nat Commun 2019;10:1–18.
36. Devaiah BN, Case-Borden C, Gegonne A, Hsu CH, Chen Q, Meerzaman D, et al. BRD4 is a histone acetyltransferase that evicts nucleosomes from chromatin. Nat Struct Mol Biol 2016;23:540.
37. Tian TV, Di Stefano B, Stik G, Vila-Casadesús M, Sardina JL, Vidal E, et al. Whsc1 links pluripotency exit with mesendoderm specification. Nat Cell Biol 2019;21:824–34.
38. Kato T, Sato N, Hayama S, Yamabuki T, Ito T, Miyamoto M, et al. Activation of holliday junction recognizing protein involved in the chromosomal stability and immortality of cancer cells. Cancer Res 2007;67:8544–53.
39. Filipescu D, Naughtin M, Podsypanina K, Lejour V, Wilson L, Gurard-Levin ZA, et al. Essential role for centromeric factors following p53 loss and oncogenic transformation. Genes Dev 2017;31:463–80.
40. Cao R, Wang G, Qian K, Chen L, Qian G, Xie C, et al. Silencing of HJURP induces dysregulation of cell cycle and ROS metabolism in bladder cancer cells via PPARgamma-SIRT1 feedback loop. J Cancer 2017;8:2282–95.
41. Wei Y, Ouyang GL, Yao WX, Zhu YJ, Li X, Huang LX, et al. Knockdown of HJURP inhibits non-small cell lung cancer cell proliferation, migration, and invasion by repressing wnt/beta-catenin signaling. Eur Rev Med Pharmacol Sci 2019;23:3847–56.
42. Chen T, Huang H, Zhou Y, Geng L, Shen T, Yin S, et al. HJURP promotes hepatocellular carcinoma proliferation by destabilizing p21 via the MAPK/ERK1/2 and AKT/GSK3β signaling pathways. J Exp Clin Cancer Res 2018; 37:193.
43. Serafim RB, Cardoso C, Di Cristofaro LFM, Soares CP, Silva WA Jr, Espreafico EM, et al. HJURP knockdown disrupts clonogenic capacity and increases radiation-induced cell death of glioblastoma cells. Cancer Gene Ther 2020;27:319–29.
44. de Oca RM, Gurard-Levin ZA, Berger F, Rehman H, Martel E, Corpet A, et al. The histone chaperone HJURP is a new independent prognostic marker for luminal a breast carcinoma. Mol Oncol 2015;9:657–74.
45. Hu Z, Huang G, Sadanandam A, Gu S, Lenburg ME, Pai M, et al. The expression level of HJURP has an independent prognostic impact and predicts the sensitivity to radiotherapy in breast cancer. Breast Cancer Res 2010;12:R18.
46. Sarai N, Nimura K, Tamura T, Kanno T, Patel MC, Heightman TD, et al. WHSC1 links transcription elongation to HIRA-mediated histone H3. 3 deposition. EMBO J 2013;32:2392–406.
47. Shen C, Ipsaro JJ, Shi J, Milazzo JP, Wang E, Roe JS, et al. NSD3-short is an adaptor protein that couples BRD4 to the CHD8 chromatin remodeler. Mol Cell 2015;60:847–59.
48. Feng Q, Zhang Z, Shea MJ, Creighton CJ, Coarfa C, Lanz R, et al. An epigenomic approach to therapy for tamoxifen-resistant breast cancer. Cell Res 2014;24:809–19.